WILEY

RESEARCH ARTICLE OPEN ACCESS

Principles for Dendritic Spine Size and Density in Human and Mouse Cortical Pyramidal Neurons

Ruth Benavides-Piccione[1,2,3] | Isabel Fernaud-Espinosa[1,2] | Asta Kastanauskaite[1,2] | Javier DeFelipe[1,2,3]

[1]Instituto Cajal (CSIC), Madrid, Spain | [2]Laboratorio Cajal de Circuitos Corticales (CTB), Universidad Politécnica de Madrid (UPM), Campus Montegancedo S/N, Pozuelo de Alarcón, Madrid, Spain | [3]Centro de Investigación Biomédica en Red sobre Enfermedades Neurodegenerativas (CIBERNED), ISCIII, Madrid, Spain

Correspondence: Ruth Benavides-Piccione (rbp@cajal.csic.es)

ABSTRACT

Dendritic spines of pyramidal neurons are the targets of most excitatory synapses in the cerebral cortex, and dendritic spine morphology directly reflects their function. However, there are scarce data available regarding both the detailed morphology of these structures for the human cerebral cortex and the extent to which they differ in comparison with other species. Thus, in the present study, we used intracellular injections of Lucifer yellow to reconstruct—in three dimensions—the morphology of basal dendritic spines from pyramidal cells in the human and mouse CA1 hippocampal region and compared these spines with those of the human temporal and cingular cortex. We found that human hippocampal dendrites show lower spine density, larger volume, and longer length of dendritic spines than mouse CA1 spines. Furthermore, human hippocampal dendrites show higher spine density, smaller spine volume, and shorter length compared to dendritic spines from the human temporal and cingular cortex. This morphological diversity suggests an equally large variability of synaptic strength and learning rules across these brain regions in humans and between humans and mice. Nevertheless, a balance between size and density was found in all cases, which may be a cortical rule maintained across cortical areas and species.

1 | Introduction

Dendritic spines (for simplicity, spines) are small protrusions that emerge from the dendrites and are the main postsynaptic targets of cortical excitatory synapses. Thus, they play a crucial role in synaptic transmission and plasticity, which are fundamental processes underlying learning and memory (Yuste 2023). Because almost all spines establish at least one excitatory glutamatergic synapse (Arellano, Espinosa, et al. 2007), variations in the number of spines within the dendritic arbors of neurons can have signif-

icant effects on both cellular and system-level cortical functions. In the neocortex, there are significant variations in the density of spines and structure of pyramidal cells in different cortical areas and species—variations that are believed to contribute to the functional differences found among such species and areas (e.g., Elston et al. 2001, 2006; Jacobs et al. 1997, 2001; Elston and Rockland 2002; Elston 2003; Bianchi et al. 2013; Benavides-Piccione et al. 2024). For instance, pyramidal cells in the granular prefrontal and temporal associational cortex of primates, including humans, exhibit a larger, more branched,

---

---

and more spinous structure compared to those found in other sensory areas (Elston et al. 2001; Jacobs et al. 1997, 2001; Elston and Rockland 2002; Elston 2003; Benavides-Piccione et al. 2024). In the mouse cortex, these variations have also been observed between regions, although to a lesser degree (Ballesteros-Yáñez et al. 2010). Indeed, the difference in spine density among cortical areas of primates, including humans, can be up to 10-fold, whereas a 2-fold difference in spine density has been reported in mouse neocortex (Jacobs and Scheibel 2002; Elston 2007; Ballesteros-Yáñez et al. 2010). Furthermore, when comparing between human and mouse, spine densities may be higher or lower depending on the cortical regions that are compared. For example, human temporal cortex shows—in general—a higher spine density than that found in the mouse cortex, whereas the mouse prelimbic cortex has a relatively higher density of spines than the human cingular cortex (Benavides-Piccione et al. 2002, 2013; Ballesteros-Yáñez et al. 2010). Nevertheless, the total number of spines per cell is usually higher in the human than in the mouse, primarily due to the larger size and branching complexity of human neurons. The increased relative compartmentalization in human neurons compared to non-human primates and rodent neurons has been examined not only from a morphological perspective but also in terms of physiology and transcriptomics (e.g., Elston et al. 2001; Beaulieu-Laroche et al. 2018; Benavides-Piccione et al. 2020; Kalmbach et al. 2021; Kanari et al. 2024). This suggests that human pyramidal neurons can generally integrate a substantially higher number of inputs than their mouse counterparts. However, this is not always the case since, for example, pyramidal neurons in the human primary visual cortex have fewer spines than pyramidal neurons in the mouse CA1 field of the hippocampus and, thus, lower compartmentalization capacity relative to CA1 rodent neurons (Benavides-Piccione et al. 2024).

Regarding spine morphology, it has been shown that the size and shape of spines are closely related to spine function. For example, the spine head volume is correlated with the area of the postsynaptic density. In turn, the size of the postsynaptic density is correlated with the number of presynaptic vesicles, the number of postsynaptic receptors, and the readily releasable pool of transmitter—and therefore with synaptic strength (Harris and Stevens 1989; Nusser et al. 1998; Schikorski and Stevens 1999, 2001; Arellano, Benavides-Piccione, et al. 2007). The length of the spine neck is proportional to the extent of biochemical and electrical isolation of the spine from its parent dendrite (Harris and Stevens 1989; Nusser et al. 1998; Schikorski and Stevens 1999, 2001; Majewska et al. 2000; Sabatini et al. 2002; Yuste and Majewska 2001; Segal 2002; Holthoff et al. 2002; Yuste and Bonhoeffer 2001; Noguchi et al. 2005; Araya et al. 2006). It has also been shown that larger spines can generate larger synaptic currents than smaller spines (Matsuzaki et al. 2004). In addition, spines are dynamic structures with fluctuations in volume that seem to have important implications for cognition and memory (Matus 2000; Bonhoeffer and Yuste 2002; Dunaevsky et al. 1999; Kasai et al. 2010; Mel et al. 2017). It has also been shown that spine necks are plastic structures that become wider and shorter after long-term potentiation (Tønnesen et al. 2014). Human spines show a variety of morphologies (Benavides-Piccione et al. 2013), which are thought to have direct functional relevance. In addition, we have previously reported the existence of systematic differences in neocortical spine head sizes and neck lengths

between humans and mouse (Benavides-Piccione et al. 2002). Nevertheless, a constraint on comparing neurons in human versus other species is the question of the homology of the cortical areas between species. Thus, in the present study we reconstructed—in three dimensions—the morphology of basal spines from pyramidal cells in the human CA1 region of the hippocampus, an evolutionarily conserved archicortical region (e.g., Stephan and Andy 1970) that is critically involved in memory formation, consolidation, and retrieval—and we then compared this morphology with that of the mouse. Furthermore, we focused on the basal dendrites of CA1 pyramidal neurons because their organization differs between rodents and humans. In rodents, the excitatory connections with the basal dendrites are mostly restricted to the *stratum oriens*, where the basal dendritic arbor is located. However, in humans, basal dendrites and apical dendrites are mostly intermingled (Benavides-Piccione et al. 2020). This means that the apical tree of one cell overlaps the basal tree of another, potentially leading to differences in the density and/or morphology of spines between the two species. In addition, we compared these spines with those of the human temporal and cingular cortex. We found that human CA1 pyramidal neurons in the two species show characteristic spine morphologies, which are different from human neocortical spines, although there does appear to be a conserved spine size-density balance.

2 | Materials and Methods

2.1 | Tissue Preparation

Samples were obtained at autopsy (1–4 h postmortem [PT]) from the Laboratorio de Neuroanatomía Humana, Facultad de Medicina, Universidad de Castilla-La Mancha, Albacete, Spain, and Instituto de Neuropatología, Servicio de Anatomía Patológica, IDIBELL-Hospital Universitario de Bellvitge, Barcelona, Spain. The tissue was obtained following national laws and international ethical and technical guidelines on the use of human samples for biomedical research purposes. Coronal sections of the human CA1 hippocampus (HCA1) at the level of the hippocampal body (Insausti and Amaral 2012) were obtained from case AB1 (male, 45 years old) and case AB2 (female, 53 years old); temporal (Brodmann's area 20; Htemp) and cingular (Brodmann's area 24; Hcing) cortex were obtained from case C40 (male, 40 years old). These cases were used as controls in previous studies (Benavides-Piccione et al. 2013, 2020, 2024). Upon removal, the brains were immersed in cold 4% paraformaldehyde in 0.1 M phosphate buffer, pH 7.4 (PB), and sectioned into thick coronal slabs to facilitate fixation. Small blocks from the regions of interest were then extracted and transferred to a second solution of 4% paraformaldehyde in PB for 24 h at 4°C. Vibratome sections (300 μm; three per individual; $n = 9$) of the HCA1 region, Htemp, and Hcing cortex were obtained in the coronal plane. Mouse tissue samples were obtained from C57BL/6 adult (8-week-old) male mice ($n = 3$; id7, id20, id10). All animals were overdosed by intraperitoneal injection of sodium pentobarbitone and perfused through the heart with 0.1 M phosphate-buffered saline followed by 4% paraformaldehyde in 0.1 M PB. The brains were then removed and further immersed in 4% paraformaldehyde for 24 h. Coronal sections (200 μm; three per case; $n = 9$) were obtained with a vibratome, which included the dorsal CA1 region (Paxinos and Franklin 2004; MCA1).
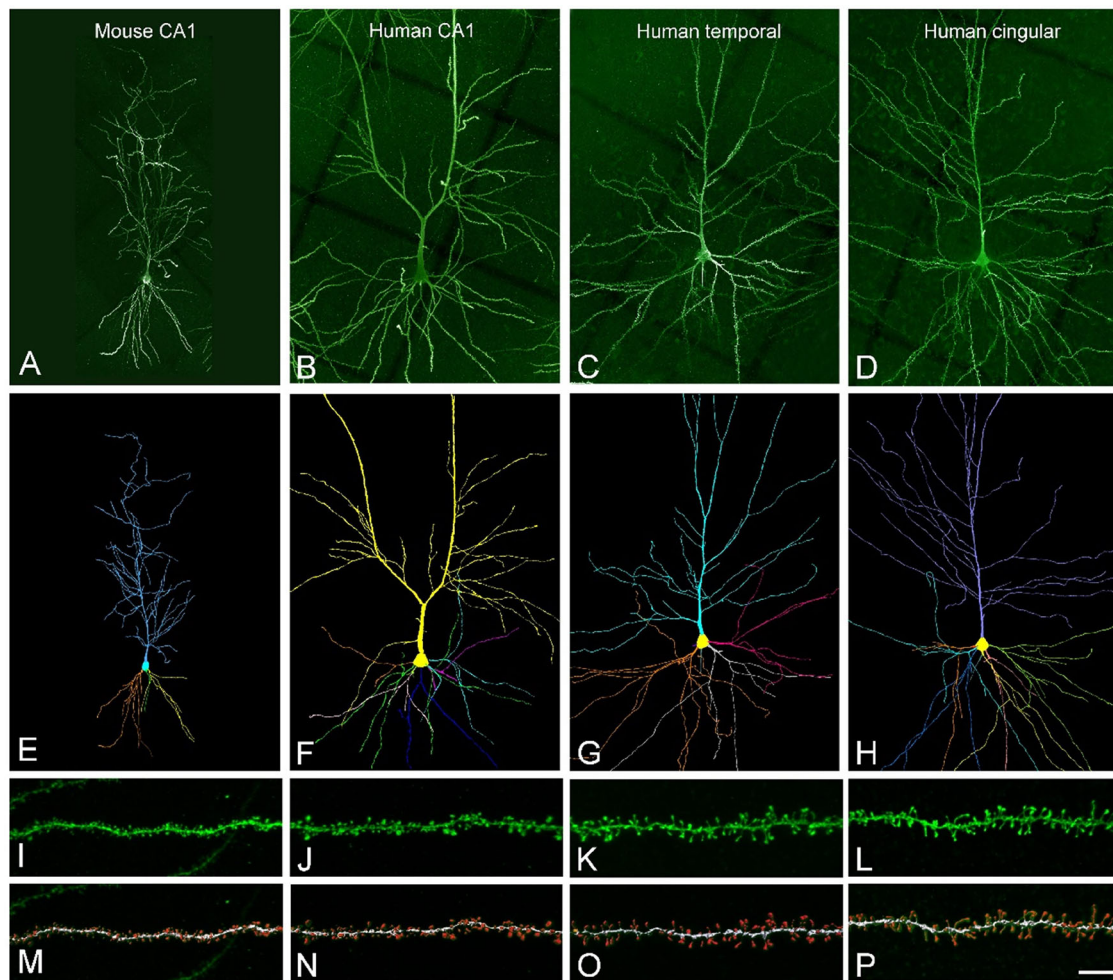
FIGURE 1 | (A–D) Confocal microscopy *z* projection images of LY-labeled pyramidal neurons in the mouse (A) and human (B) CA1 field of the hippocampal formation and the human temporal (C) and cingular (D) cortex. (E–H) 3D reconstruction of the same cells shown in A–D. (I–L) High-magnification confocal microscopy images showing labeled basal dendritic segments in the mouse (I) and human (J) CA1 field of the hippocampal formation and the human temporal (K) and cingular (L) cortex. (M–P) Each spine and shaft was 3D reconstructed by selecting a particular threshold that represented a solid surface that matched the contour of the spine (red) and shaft (white). Scale bar (in P) = 50 μm in A–H and 6 μm in I–P.

2.2 | Intracellular Injections and Immunocytochemistry

Human and mouse sections were labeled with 4,6-diamidino-2-phenylindole (DAPI; Sigma, St. Louis, MO) to identify cell bodies. Continuous current was used to inject individual cells with Lucifer yellow (LY; 8% in 0.1 M Tris buffer, pH 7.4) in the pyramidal cell layer of the CA1 field of the human and mouse hippocampus and in layer IIIa of the human temporal and cingular cortex (Figure 1). LY was applied to each injected cell by continuous current until the distal tips of each cell fluoresced brightly, indicating that the dendrites were completely filled and ensuring that the fluorescence did not diminish at a distance from the soma. Following the intracellular injections, the sections were immunostained for LY using rabbit antisera against LY (1:400,000; generated at the Cajal Institute) diluted in stock solution (2% bovine serum albumin, 1% Triton X-100, and 5% sucrose in PB). The sections were then incubated in biotinylated donkey anti-rabbit IgG (1:100; Amersham, Buckinghamshire, United Kingdom) and streptavidin-conjugated Alexa Fluor 488 (1:1000; Molecular Probes, Eugene, OR, USA). Finally,

the sections were washed and mounted with either ProLong Gold Antifade Reagent (Invitrogen Corporation, Carlsbad, CA, USA) or glycerol 50% in PB. See Benavides-Piccione et al. (2013, 2020) for further details of the cell injection methodology.

2.3 | Imaging and Quantitative Analysis

The sections were imaged with a Leica TCS 4D confocal scanning laser attached to a Leitz DMIRB fluorescence microscope. Fluorescent labeling profiles were imaged using an excitation wavelength of 491 nm to visualize Alexa Fluor 488. Horizontally projecting basal dendrites were randomly selected, each one originating from a different pyramidal neuron (10 per group; $n = 40$). Consecutive stacks of images (2–4 per dendrite; $n = 110$) were acquired at high magnification (63× glycerol; zoom factor, 2.3; voxel size, $0.075 \times 0.075 \times 0.28$ μm in the human and $0.075 \times 0.075 \times 0.14$ μm in the mouse) to capture the full depth, length, and width of the basal dendrites from the soma to their distal tips. For each stack of images, confocal parameters were

set so that the fluorescence signal was as bright as possible while ensuring that there were no pixels saturated within the spines.

Spine density was determined by counting the number of spines per 10 μm of dendritic length, starting at the soma and continuing to the distal tips of the basal dendrites from the Htemp cortex. Spine density values from Hcing cortex were taken from Benavides-Piccione et al. (2013), whereas those from the HCA1 and MCA1 regions were taken from Benavides-Piccione et al. (2024), in which the same methodology was used. Although spine density in Htemp had already been analyzed in that study, we reanalyzed spine density in the present study using dendrites from a different human case (the same case used for the Hcing analysis) to minimize interindividual variability, as significant variation in spine density is known to exist between human individuals (Benavides-Piccione et al. 2021). All spines were included and considered equally in the analysis. Correction factors that were used in other studies when quantifying spines with the Golgi method (e.g., Feldman and Peters 1979) were not used in the present study as the fluorescent labeling and the high-power reconstruction allowed the visualization of spines that protrude from the underside of dendrites.

Spine structure was analyzed using Imaris 6.4.0 (Bitplane AG, Zurich, Switzerland). We reconstructed the complete morphology of each spine per dendrite in 3D from the MCA1, HCA1, and Htemp regions to capture its volume and length (1467–3133 spines per group; $n = 9176$). Spine values from the Hcing region were taken from Benavides-Piccione et al. (2013), in which the same methodology was used. However, confocal stacks of images intrinsically result in a z-dimension distension; thus, a correction factor of 0.84 was applied to this dimension. This factor was calculated using a 4.2 μm TetraSpeck Fluorescent microsphere (Molecular Probes, Eugene, OR) using the same parameters as those employed for the acquisition of dendritic stacks. By comparing the surface area obtained with the microscope with the theoretical calculated area of the identified sphere, we calculated the corresponding correction factor (see Benavides-Piccione et al. 2013). To capture *spine volume*, we generated 7–10 different intensity threshold surfaces using Imaris software. As previously published (Benavides-Piccione et al. 2013), the different intensity threshold surfaces generated allowed us to capture the complete range of sizes. Then, for each individual spine, we manually selected the particular threshold that constituted a solid surface that exactly matched the contour of each spine (Figures 1 and 2) along the length of the dendrites. However, it was sometimes necessary to merge several surfaces from different intensity thresholds to capture the complete morphology of a spine (see Figure 2C). That is, because sometimes the different parts of the spine showed quite different fluorescent intensity (i.e., head vs. neck), we sometimes had to select specific surfaces that were generated from different intensity thresholds in order to be able to reconstruct the complete morphology of the spine. *Spine length* was manually marked in each individual spine, from its point of insertion in the dendritic shaft to the distal tip of the spine (Figure 2E), while rotating the image in three dimensions. Using the same method to the one employed previously for modeling the human temporal and cingular cortex (Eyal et al. 2016), here we computed the *F factor* for the MCA1 and HCA1 regions. This factor is defined by (dendritic membrane area + total spine area)/dendritic membrane area. The *F* factor refers—in a particular dendrite—to the % of the dendritic membrane area that belongs to spines (Figures 1M–P and 2B). The *F* factor was computed for human dendrites in those segments that were at a distance of at least 60 μm from the soma, due to the very small density of spines in the more proximal branches (Benavides-Piccione et al. 2013). For mouse dendrites, the *F* factor was computed in those segments that were at a distance of at least 30 μm from the soma for the same reason.

In addition, we measured the *spine head surface area, spine neck length, and spine neck diameter* in a selection of 150–215 spines per group. We visually identified individual spines that exhibited a clearly distinguishable head and neck morphology, as illustrated in Figure 2D–H. The spine head surface area, neck length and neck diameter were measured in each selected spine using a similar methodology to that used for the spine reconstruction, in the MCA1, HCA1, and Hcing regions. Spine head surface area, spine neck length, and spine neck diameter values from the Htemp region were taken from Eyal et al. (2018), in which the same methodology and human case were used. Regarding spine neck diameter, three different measurements (neck diameter 1, 2, and 3) were additionally taken in MCA1, HCA1, Hcing, and Htemp regions due to possible variations from the point of insertion in the dendritic shaft to the spine head (Figure 2I). The analysis of all spine variables was performed under blinded conditions.

2.4 | Statistics

All statistical analyses were performed using GraphPad Prism version 9.3.1 for Windows (GraphPad Software, San Diego, California, USA). When morphological parameters were presented as mean values per dendrite and frequency distributions, Kruskal–Wallis and Kolmogorov–Smirnov tests were used, respectively, to compare between the groups. Measurements reported as a function of the distance from soma were analyzed using repeated-measures analysis of variance and Tukey's multiple comparison tests. Measurements are reported as mean ± *SEM* unless otherwise indicated.

3 | Results

Over 9000 spines were analyzed along the pyramidal cell basal dendrites from human and mouse CA1 hippocampal field, human temporal, and human cingular cortex (HCA1, MCA1, Htemp, and Hcing, respectively). Figure 3A shows that HCA1 dendrites exhibited significantly higher spine density than Htemp and Hcing dendrites (Tables 1 and S1), whereas MCA1 dendrites had the highest density. Both neocortical regions showed similar spine density values. The spine distribution—presented as a frequency (Figure 3B, Table S2) and as a distribution along the length of dendrites (Figure 3C; Table S3)—showed that Htemp and Hcing were the most similar groups. In all groups, spine density gradually increased along dendrites, reaching a peak at approximately 90–110 μm from the soma, and then gradually decreased toward the distal end of the dendrite. Significant
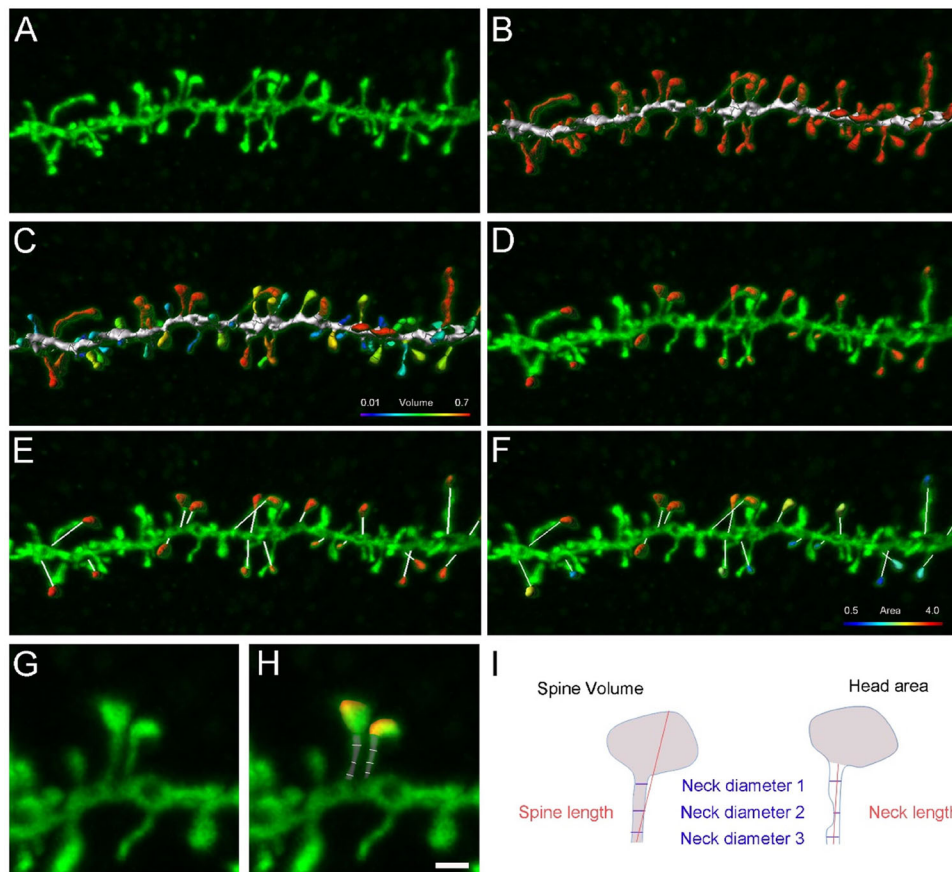
FIGURE 2 | (A–F) High-magnification confocal microscopy images showing an example of a labeled cingular basal dendritic segment in (A) to illustrate the 3D reconstruction of (B) spines (red) and shaft (white), (C) spines color coded by size (volume: blue-red: 0.01 - 0.7 μm^3) and shaft (white), (D and E) selected spine heads (red) and neck lengths (white lines), and (F) selected spine heads shown in D color coded by size (area: blue-red: 0.5 - 4.0 μm^2) and neck lengths shown in E. (G and H) Higher magnification images to illustrate neck diameter measurements. (I) Schematic of spine variables analyzed. Scale bar (in H) = 2 μm in A–F and 0.7 μm in G and H.

differences were found in all cases except between the Htemp and Hcing cortical regions (Figure 3C and Table S3).

Regarding spine volumes, HCA1 spines were significantly smaller than Htemp and Hcing spines, whereas MCA1 spines were the smallest (Figure 3D and Tables 1 and S1). Htemp spines were also significantly larger than Hcing spines. The study of their distributions (Figure 3E and Table S2) revealed significant differences between mouse and some human groups. In addition, spine volumes were analyzed as a function of the distance from soma, showing that spines in the Htemp and Hcing regions were larger than those in the MCA1 and HCA1 regions, particularly in the proximal segment up to 70 μm (Figure 3F; Table S3 for statistical comparisons). Furthermore, we found no significant differences between the distribution of Htemp and Hcing dendrites.

Spines from HCA1 were shorter than Htemp and Hcing spines, whereas those in MCA1 mouse dendrites were the shortest (Figure 3G and Tables 1 and S1). Htemp spines were also significantly longer than Hcing spines. The value distributions (Figure 3H) showed significant differences between mouse and some human groups (Table S2). Spine lengths, when analyzed as a function of the distance from the soma, showed statistically significant differences at some distances (Figure 3I; see Table S3 for statistical comparisons). Htemp and Hcing distribution comparisons yielded similar values.

We then measured the spine head area, spine neck length, and spine neck diameter in a subset of 150–215 spines per group that were selected because they showed typical spine morphology in which the spine head could be clearly distinguished. The results showed that MCA1 spines had the smallest heads, as well as the shortest and thinnest necks, whereas Htemp and Hcing showed the largest values (Figure 4, Table 1, and Table S1). No significant differences were found for either neck lengths or neck diameters of typical spines when measurements between the Htemp and Hcing regions were compared.

Finally, we computed the percentage of the dendritic membrane area corresponding to spines in each dendrite by using the F factor (see Section 2 for further details as well as Figures 1M–P and 2B). We computed the F factor for the MCA1 and HCA1 regions using a similar approach to the one employed previously for the modeling of the human temporal and cingular cortex (Eyal et al. 2016). We found that the F factor was around 2 in all cases (Table 1), indicating that half of the total membrane area is covered by spines, despite the great variations in density and size.
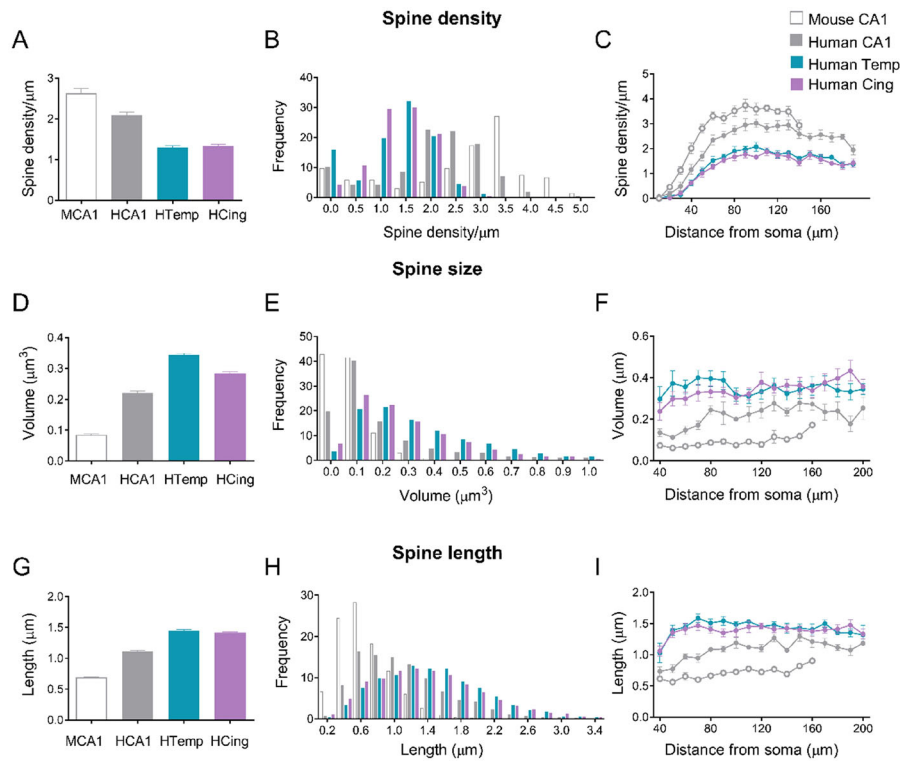
FIGURE 3 | Graphs showing spine density (A–C), spine volume (D–F), and spine length (G–I) as mean values (A, D, G), frequency distribution (B, E, H), and as a function of the distance from soma (C, F, I) for the basal dendrites from mouse and human CA1 region and human temporal and cingular cortical areas. Measurements are reported as mean ± *SEM*. The statistical significance of the differences is shown in Tables S1–S3. *Source:* (A–C) Spine density values from CA1 regions were taken from Benavides-Piccione et al. (2024), and values from the Hcing region were taken from Benavides-Piccione et al. (2013). (D–I) Spine volume and length values from the Hcing region were taken from Benavides-Piccione et al. (2013).

TABLE 1 | Mean ± *SEM* values per variable and cortical region.

	Mean ± *SEM*			
	MCA1	**HCA1**	**Htemp**	**Hcing**
Spine density (μm)	2.624 ± 0.120[a]	2.094 ± 0.072[a]	1.290 ± 0.046	1.340 ± 0.039[a]
Spine volume (μm³)	0.085 ± 0.002	0.220 ± 0.007	0.344 ± 0.005	0.284 ± 0.004[a]
Spine length (μm)	0.689 ± 0.008	1.115 ± 0.014	1.449 ± 0.012	1.417 ± 0.013[a]
Spine head surface area (μm²)[b]	0.833 ± 0.037	1.704 ± 0.089	2.885 ± 0.112[a]	2.037 ± 0.071
Spine neck length (μm)[b]	0.523 ± 0.016	0.888 ± 0.027	1.344 ± 0.041[a]	1.314 ± 0.056
Spine neck mean diameter (μm)[b]	0.117 ± 0.002	0.165 ± 0.003	0.242 ± 0.006[a]	0.219 ± 0.005
Spine neck diameter 1 (μm)[b]	0.124 ± 0.002	0.172 ± 0.003	0.262 ± 0.007	0.221 ± 0.006
Spine neck diameter 2 (μm)[b]	0.107 ± 0.002	0.159 ± 0.003	0.205 ± 0.007	0.209 ± 0.006
Spine neck diameter 3 (μm)[b]	0.119 ± 0.002	0.165 ± 0.005	0.259 ± 0.007	0.228 ± 0.006
F factor	$F = 2.13 \pm 0.10$	$F = 2.09 \pm 0.15$	$F = 2.39 \pm 0.20$[a]	$F = 1.98 \pm 0.12$[a]

[a]Previously published (see Section 2 for details).
[b]See methodological considerations.

Spine head surface area

Spine neck length
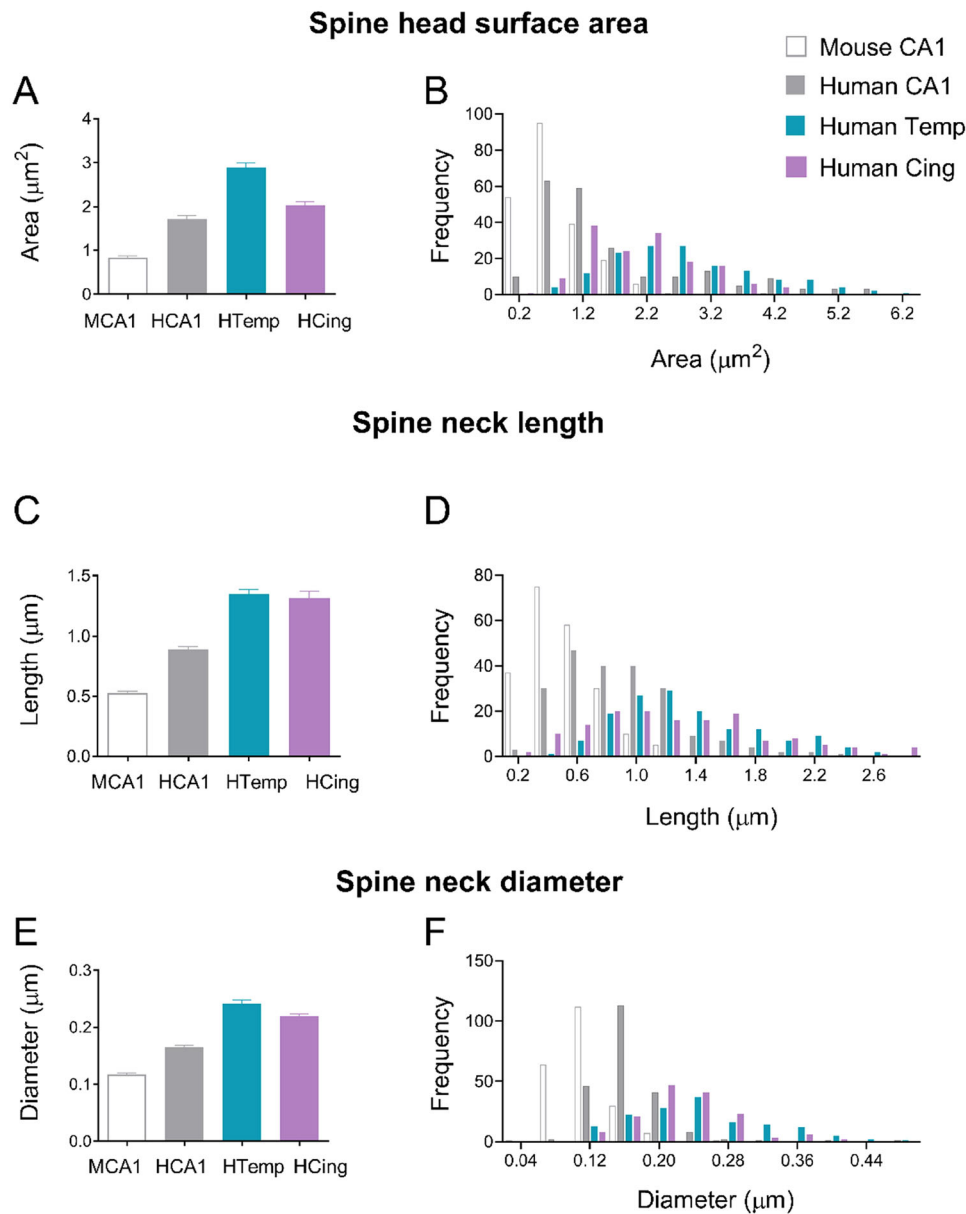

Spine neck diameter

FIGURE 4 | Graphs showing spine head area (A and B), spine neck length (C and D), and spine neck diameter (E and F) as mean values (A, C, E) and frequency distribution (B, D, F) for the basal dendrites from mouse and human CA1 region and human temporal and cingular cortical areas. Measurements are reported as mean ± *SEM*. The statistical significance of the differences is shown in Tables S1 and S2. *Source:* Spine values from the Htemp region were taken from Eyal et al. (2018).

4 | Discussion

The main finding in the present study is that CA1 pyramidal neurons in humans and mice exhibit distinct spine morphologies—also differing from those observed in the human temporal and cingular cortex. Specifically, human CA1 dendrites display lower spine density, larger spine volume, and longer spine length compared to mouse CA1 dendrites. Furthermore, human CA1 dendrites exhibit higher spine density, smaller spine volume, and shorter spine length compared to dendrites from the human temporal and cingular cortex, which, in turn, are relatively similar to each other. Finally, despite these differences, there is a cortical dendritic spine size-density balance between regions and species.

4.1 | Methodological Considerations

One potential caveat to consider is the comparison of PT tissue fixed by immersion (human cases) with perfusion-fixed brain tissue with no PT delay (mouse cases). Our previous study (Gonzalez-Riano et al. 2017), which examined PT-induced changes in metabolomic and anatomical markers in mouse brains, found significant metabolomic alterations starting at 2 h PT, whereas the structural integrity of neurons and glia was largely preserved for most histological markers within the first 5 h PT. However, since this 2017 study did not assess the PT effects on spines, we could not rule out the possibility that some of the observed differences may have been the result of technical factors. Nonetheless, in an earlier study (Benavides-Piccione et al. 2002),

we directly examined the potential impact of fixation method (perfusion vs. immersion) on spine morphology and density in mice. In that experiment, one mouse hemisphere was fixed by immersion using the same protocol applied to human tissue, and the results were compared to perfusion-fixed tissue from the same cortical region. We found that spine density and size were indistinguishable between the two conditions. On the basis of these findings, we are confident that the present results are methodologically robust and that the fixation differences are unlikely to account for the reported observations.

Regarding sampling, although we analyzed thousands of individual three-dimensionally reconstructed spines, the overall sample size was limited to brain tissue from only three human individuals. This limitation arose from the difficulties associated with obtaining tissue with an optimal quality of fixation and preservation, which is crucial for detailed studies of complete spine morphology. Additionally, human brains exhibit remarkable interindividual variability (e.g., DeFelipe 2011; Benavides-Piccione et al. 2021). Furthermore, previous studies have demonstrated age-related changes in dendritic spines, including a significant reduction in spine density and alterations in spine volume (e.g., Dumitriu et al. 2010; Benavides-Piccione et al. 2013; Motley et al. 2018). In the present study, we compared middle-aged human tissue with tissue from 2-month-old mice, and these age differences may have contributed to amplifying the interspecies differences observed in spine parameters. Future studies incorporating age-matched comparisons across species would be valuable to more accurately assess these differences. Additionally, the spine head area, spine neck length, and spine neck diameter were measured exclusively in a subset selection of "typical" spines exhibiting a distinct head for modeling purposes. Thus, with a larger and more diverse sample size, the findings might be more generalizable to the whole population. Nevertheless, it is important to bear in mind that the human cerebral cortex is unique in many respects, including genetic, molecular, structural, and physiological aspects. Therefore, research on human brain is fundamental in spite of these limitations. In other words, this study represents a further step toward the characterization of human brain microorganization, but it would be necessary to confirm these findings with a larger number of individuals and cortical regions, while also including a more diverse sample of dendrites as well as incorporating apical dendritic arbors. The main findings of this study will now be discussed in the sections that follow.

4.2 | Human and Mouse Hippocampal Pyramidal Neurons Show Higher Spine Density Than Human Temporal and Cingular Neurons

Human CA1 dendrites had significantly higher spine density than those in the human temporal and cingular cortex. Differences in spine densities across species have been reported previously (e.g., Elston et al. 2001; Jacobs et al. 2001; Gilman et al. 2017; Benavides-Piccione et al. 2024), and our results confirm and extend these findings. In particular, an analysis of spine density comparing the hippocampal regions and the human temporal cortex had also previously been carried out, but the samples came from other individuals (Benavides-Piccione et al. 2024). In spite of the human interindividual variability found in spine density from the temporal cortex (Benavides-Piccione et al. 2021),

all values from the different individuals analyzed in the present and previous studies showed that spine density in the CA1 field was consistently higher than that in the temporal cortex. Because cells from both human regions are similar in size and dendritic branching complexity (Benavides-Piccione et al. 2024), this implies that the higher density of spines in HCA1 would be associated with differences between the number of excitatory inputs the two regions can integrate. The larger number of synaptic inputs in HCA1 cells suggests a greater potential for synaptic input and integration of information compared to Htemp cells. This increased connectivity can influence the ability to participate in more complex and diverse cortical circuits and information processing tasks. Similarly, although pyramidal cells in MCA1 are relatively small and have less complex dendritic arbors than HCA1 cells (Benavides-Piccione et al. 2024), the very high density of spines endows these cells with a relatively high potential for the integration of information and enhanced synaptic connectivity compared to other mouse neocortical regions (Ballesteros-Yáñez et al. 2010).

4.3 | Human and Mouse CA1 Dendrites Show Higher Proportion of Small and Short Spines Compared to Human Temporal and Cingular Dendrites

Regarding spine volume and length, HCA1 spines were significantly smaller and shorter than Htemp and Hcing spines, whereas MCA1 spines were the smallest. The Htemp and Hcing cortical regions were more similar to each other than other region comparisons, although Htemp showed higher mean spine volume and length values. Regarding spine compartments, the Htemp region had the largest spine heads and thickest spine necks, whereas mouse CA1 spines had the smallest heads with the shortest and thinnest necks. It is thought that small spines are preferential sites for long-term potentiation induction, whereas large spines might represent physical traces of long-term memory (Matsuzaki et al. 2004; Kasai et al. 2010). Thus, it is possible that the increased prevalence of small spines observed in hippocampal dendrites might correlate with a greater potential for plasticity in the CA1 region compared to temporal and cingular cortex. This aligns well with the CA1's established role in memory formation. Conversely, the relatively lower percentage of small spines in temporal and cingular dendrites could suggest a lesser potential for plasticity in these dendrites.

The variations in spine length are related to changes in biochemical compartmentalization (reviewed in Yuste 2023). Thus, the long necks found in the human temporal and cingular cortex likely isolate the spine from its parent dendrite to a larger extent than hippocampal spines, both in the mouse and the human. Interestingly, because spine necks are plastic structures that become wider and shorter after long-term potentiation (Tønnesen et al. 2014), the similar neck length values found in the Htemp and Hcing regions, together with the larger Htemp spine head and neck diameters, could imply an enhanced capability to support long-term memory in the case of temporal spines. Conversely, the relatively smaller Hcing spine head size, related to the excitatory postsynaptic potential (EPSP), may correspond to a decrease in the electrical response of the spine's head when excitatory neurotransmitters are released.

4.4 | There Is a Continuum of Variability of Spine Sizes

The frequency distribution of spine sizes (including spine volume, length, head area, neck length, and neck diameter) showed a continuum of variability in all cases. This was also found in previous studies (e.g., Spacek and Hartmann 1983; Harris et al. 1992; Benavides-Piccione et al. 2002; Ballesteros-Yáñez et al. 2006; Arellano, Benavides-Piccione, et al. 2007). Importantly, a differential distribution of values was found in human neocortex compared to the human CA1 region. The larger proportion of diverse spine sizes found in Htemp and Hcing suggests a larger variability of synaptic strengths (Yuste 2023) compared to the hippocampal regions.

4.5 | Distinct Distribution Pattern of Spines Along the Distance From the Soma

In line with findings from previous studies conducted across various species and cortical regions (Elston et al. 2001; Elston and DeFelipe 2002; Ballesteros-Yáñez et al. 2010; Benavides-Piccione et al. 2021, 2024), the distribution of spine density along the distance from soma, reaching a peak at approximately one-third of the total dendritic length and then slightly decreasing toward the distal tips, was remarkably similar between groups despite differences in the absolute numbers. This aligns with previous predictions on how variations in spine distribution at specific locations influence signal generation (e.g., Katz et al. 2009; Harnett et al. 2012). Moreover, basal dendrites from Htemp and Hcing showed increasing spine volume and length values for the first ~60 μm of dendritic length, which corresponds to the region where the dendrite bifurcates (Benavides-Piccione et al. 2013). Values then remained—in general—relatively similar along the remaining dendritic length. That is, because nodes are typically located approximately within the first 60 μm from the soma (with a peak at 40 μm; Benavides-Piccione et al. 2013, 2024), the distribution of spine size and length may depend on variations in dendritic diameter across branch orders. Thus, this suggests that dendritic diameter might act as a key regulatory factor in shaping spine morphology in both the Htemp and Hcing regions. By contrast, the CA1 field, for both human and mouse dendrites, showed a trend for a slight increase in spine volume and length with increasing distance from soma. Because nodes in the HCA1 and MCA1 regions also exhibit peaks at 40 and 30 μm, respectively (Benavides-Piccione et al. 2024), the distributions of these variables in the HCA1 region may depend on alternative key regulatory factors. This pattern might be a compensatory mechanism to counteract the filtering effect of long dendrites on electrical signals. It is important to note that the previous research on the neocortex of mice has also reported a lack of correlation between the spine volume and the distance from soma (Konur et al. 2003; Arellano, Benavides-Piccione, et al. 2007). However, studies in other brain regions—such as the CA1 of mice and rats, the somatic sensory cortex of cats and mice, and the primary visual cortex of mice—reported an increasing trend (e.g., Jones and Powell 1969; Konur et al. 2003; Megias et al. 2001). These observations suggest a potential regional variation in how spine morphology relates to the distance from the soma. Further research using standardized methods across different brain regions is necessary to substantiate this hypothesis.

4.6 | Conserved Cortical Spine Size-Density Balance

Despite differences in spine size and density between regions and species, the analysis of the percentage of spine area relative to the total dendritic membrane area (*F* factor) showed that, in all groups, around half of the total membrane area is covered with spines. Furthermore, dendritic diameters from Htemp, Hcing, and HCA1 basal dendrites are relatively similar to each other and thicker than MCA1 basal dendrites (Benavides-Piccione et al. 2013, 2024, and unpublished observations). Thus, there may be a balance between spine size and density relative to the diameter of the dendrite that may be a cortical rule maintained across cortical areas and species.

In summary, taking together the previous data and the present results, it is clear that CA1 pyramidal cells exhibit a relatively higher capability of integrating information compared to neocortical cells. Moreover, the relatively higher proportion of small and short spines found in CA1 dendrites suggests a higher number of preferential sites for long-term potentiation and, consequently, a greater capacity for learning and memory in the hippocampal region compared to the temporal and cingular regions. Furthermore, the human temporal and cingular regions, with their greater morphological diversity, may have a greater diversity of synaptic strengths compared to hippocampal dendrites. Interestingly, despite these differences in spine features between species and areas, there is a conserved percentage of total spine area relative to the total dendritic membrane area. Future research using larger and more diverse samples could further support the connection between these morphological observations and the functional roles of these brain regions in different species.

Data Availability Statement

The data that support the findings of this study are available on request from the corresponding author. The data are not publicly available due to privacy or ethical restrictions.

Peer Review

The peer review history for this article is available at https://publons.com/publon/10.1002/cne.70060.

References

Araya, R., J. Jiang, K. B. Eisenthal, and R. Yuste. 2006. "The Spine Neck Filters Membrane Potentials." *Proceedings of the National Academy of Sciences of the United States of America* 103: 17961–17966.

Arellano, J. I., R. Benavides-Piccione, J. DeFelipe, and R. Yuste. 2007. "Ultrastructure of Dendritic Spines: Correlation Between Synaptic and Spine Morphologies." *Frontiers in Neuroscience* 1, no. 1: 131–143. https://www.frontiersin.org/articles/10.3389/neuro.01.1.1.010.2007.

Arellano, J. I., A. Espinosa, A. Fairén, R. Yuste, and J. DeFelipe. 2007. "Non-Synaptic Dendritic Spines in Neocortex." *Neuroscience* 145: 464–469.

Ballesteros-Yáñez, I., R. Benavides-Piccione, J.-P. Bourgeois, J.-P. Changeux, and J. DeFelipe. 2010. "Alterations of Cortical Pyramidal Neurons in Mice Lacking High-Affinity Nicotinic Receptors." *Proceedings of the National Academy of Sciences of the United States of America* 107: 11567–11572.

Ballesteros-Yáñez, I., R. Benavides-Piccione, G. N. Elston, R. Yuste, and J. DeFelipe. 2006. "Density and Morphology of Dendritic Spines in Mouse Neocortex." *Neuroscience* 138: 403–409.

Beaulieu-Laroche, L., E. H. S. Toloza, M.-S. van der Goes, et al. 2018. "Enhanced Dendritic Compartmentalization in Human Cortical Neurons." *Cell* 175: 643–651.e14.

Benavides-Piccione, R., I. Ballesteros-Yáñez, J. DeFelipe, and R. Yuste. 2002. "Cortical Area and Species Differences in Dendritic Spine Morphology." *Journal of Neurocytology* 31: 337–346.

Benavides-Piccione, R., L. Blazquez-Llorca, A. Kastanauskaite, I. Fernaud-Espinosa, S. Tapia-González, and J. DeFelipe. 2024. "Key Morphological Features of Human Pyramidal Neurons." *Cerebral Cortex* 34: bhae180.

Benavides-Piccione, R., I. Fernaud-Espinosa, V. Robles, R. Yuste, and J. DeFelipe. 2013. "Age-Based Comparison of Human Dendritic Spine Structure Using Complete Three-Dimensional Reconstructions." *Cerebral Cortex* 23: 1798–1810.

Benavides-Piccione, R., M. Regalado-Reyes, I. Fernaud-Espinosa, et al. 2020. "Differential Structure of Hippocampal CA1 Pyramidal Neurons in the Human and Mouse." *Cerebral Cortex* 30: 730–752.

Benavides-Piccione, R., C. Rojo, A. Kastanauskaite, and J. DeFelipe. 2021. "Variation in Pyramidal Cell Morphology Across the Human Anterior Temporal Lobe." *Cerebral Cortex* 31: 3592–3609.

Bianchi, S., C. D. Stimpson, A. L. Bauernfeind, et al. 2013. "Dendritic Morphology of Pyramidal Neurons in the Chimpanzee Neocortex: Regional Specializations and Comparison to Humans." *Cerebral Cortex* 23: 2429–2436.

Bonhoeffer, T., and R. Yuste. 2002. "Spine Motility. Phenomenology, Mechanisms, and Function." *Neuron* 35: 1019–1027.

DeFelipe, J. 2011. "The Evolution of the Brain, the Human Nature of Cortical Circuits, and Intellectual Creativity." *Frontiers in Neuroanatomy* 5: 29.

Dumitriu, D., J. Hao, Y. Hara, et al. 2010. "Selective Changes in Thin Spine Density and Morphology in Monkey Prefrontal Cortex Correlate With Aging-Related Cognitive Impairment." *Journal of Neuroscience* 30: 7507–7515.

Dunaevsky, A., A. Tashiro, A. Majewska, C. Mason, and R. Yuste. 1999. "Developmental Regulation of Spine Motility in the Mammalian Central Nervous System." *Proceedings of the National Academy of Sciences of the United States of America* 96: 13438–13443.

Elston, G. N. 2003. "Cortex, Cognition and the Cell: New Insights Into the Pyramidal Neuron and Prefrontal Function." *Cerebral Cortex* 13: 1124–1138.

Elston, G. N. 2007. "Specialization of the Neocortical Pyramidal Cell During Primate Evolution." In *Evolution of Nervous Systems*, edited by J. H. Kaas, 191–242. Academic Press. https://www.sciencedirect.com/science/article/pii/B0123708788001646.

Elston, G. N., R. Benavides-Piccione, and J. DeFelipe. 2001. "The Pyramidal Cell in Cognition: A Comparative Study in Human and Monkey." *Journal of Neuroscience* 21: RC163.

Elston, G. N., R. Benavides-Piccione, A. Elston, et al. 2006. "Specializations of the Granular Prefrontal Cortex of Primates: Implications for Cognitive Processing." *Anatomical Record. Part A, Discoveries in Molecular, Cellular, and Evolutionary Biology* 288: 26–35.

Elston, G. N., and J. DeFelipe. 2002. "Spine Distribution in Cortical Pyramidal Cells: A Common Organizational Principle Across Species." *Progress in Brain Research* 136: 109–133.

Elston, G. N., and K. S. Rockland. 2002. "The Pyramidal Cell of the Sensorimotor Cortex of the Macaque Monkey: Phenotypic Variation." *Cerebral Cortex* 12: 1071–1078.

Eyal, G., M. B. Verhoog, G. Testa-Silva, et al. 2016. "Unique Membrane Properties and Enhanced Signal Processing in Human Neocortical Neurons." *Elife* 5: e16553.

Eyal, G., M. B. Verhoog, G. Testa-Silva, et al. 2018. "Human Cortical Pyramidal Neurons: From Spines to Spikes via Models." *Frontiers in Cellular Neuroscience* 12: 181.

Feldman, M. L., and A. Peters. 1979. "A Technique for Estimating Total Spine Numbers on Golgi-Impregnated Dendrites." *Journal of Comparative Neurology* 188: 527–542.

Gilman, J. P., M. Medalla, and J. I. Luebke. 2017. "Area-Specific Features of Pyramidal Neurons—A Comparative Study in Mouse and Rhesus Monkey." *Cerebral Cortex* 27: 2078–2094.

Gonzalez-Riano, C., S. Tapia-González, A. García, A. Muñoz, J. DeFelipe, and C. Barbas. 2017. "Metabolomics and Neuroanatomical Evaluation of Post-Mortem Changes in the Hippocampus." *Brain Structure and Function* 222: 2831–2853.

Harnett, M. T., J. K. Makara, N. Spruston, W. L. Kath, and J. C. Magee. 2012. "Synaptic Amplification by Dendritic Spines Enhances Input Cooperativity." *Nature* 491: 599–602.

Harris, K. M., F. E. Jensen, and B. Tsao. 1992. "Three-Dimensional Structure of Dendritic Spines and Synapses in Rat Hippocampus (CA1) at Postnatal Day 15 and Adult Ages: Implications for the Maturation of Synaptic Physiology and Long-Term Potentiation." *Journal of Neuroscience* 12: 2685–2705.

Harris, K. M., and J. K. Stevens. 1989. "Dendritic Spines of CA 1 Pyramidal Cells in the Rat Hippocampus: Serial Electron Microscopy With Reference to Their Biophysical Characteristics." *Journal of Neuroscience* 9: 2982–2997.

Holthoff, K., D. Tsay, and R. Yuste. 2002. "Calcium Dynamics of Spines Depend on Their Dendritic Location." *Neuron* 33: 425–437.

Insausti, R., and D. G. Amaral. 2012. "Hippocampal Formation." In *The Human Nervous System*. 3rd ed., edited by J. K. Mai and G. Paxinos, 896–942. Academic Press.

Jacobs, B., L. Driscoll, and M. Schall. 1997. "Life-Span Dendritic and Spine Changes in Areas 10 and 18 of Human Cortex: A Quantitative Golgi Study." *Journal of Comparative Neurology* 386: 661–680.

Jacobs, B., M. Schall, M. Prather, et al. 2001. "Regional Dendritic and Spine Variation in Human Cerebral Cortex: A Quantitative Golgi Study." *Cerebral Cortex* 11: 558–571.

Jacobs, B., and A. B. Scheibel. 2002. "Regional Dendritic Variation in Primate Cortical Pyramidal Cells." In *Cortical Areas: Unity and Diversity*, edited by A. Schüz and R. Miller, 111–131. Taylor & Francis.

Jones, E. G., and T. P. Powell. 1969. "Morphological Variations in the Dendritic Spines of the Neocortex." *Journal of Cell Science* 5: 509–529.

Kalmbach, B. E., R. D. Hodge, N. L. Jorstad, et al. 2021. "Signature Morpho-Electric, Transcriptomic, and Dendritic Properties of Human Layer 5 Neocortical Pyramidal Neurons." *Neuron* 109: 2914–2927.e5.

Kanari, L., Y. Shi, A. Arnaudon, et al. 2024. "Of Mice and Men: Dendritic Architecture Differentiates Human From Mice Neuronal Networks." bioRxiv [Preprint]. https://doi.org/10.1101/2023.09.11.557170.

Kasai, H., M. Fukuda, S. Watanabe, A. Hayashi-Takagi, and J. Noguchi. 2010. "Structural Dynamics of Dendritic Spines in Memory and Cognition." *Trends in Neurosciences (TINS)* 33: 121–129.

Katz, Y., V. Menon, D. A. Nicholson, Y. Geinisman, W. L. Kath, and N. Spruston. 2009. "Synapse Distribution Suggests a Two-Stage Model of Dendritic Integration in CA1 Pyramidal Neurons." *Neuron* 63: 171–177.

Konur, S., D. Rabinowitz, V. L. Fenstermaker, and R. Yuste. 2003. "Systematic Regulation of Spine Sizes and Densities in Pyramidal Neurons." *Journal of Neurobiology* 56: 95–112.

Majewska, A., E. Brown, J. Ross, and R. Yuste. 2000. "Mechanisms of Calcium Decay Kinetics in Hippocampal Spines: Role of Spine Calcium Pumps and Calcium Diffusion Through the Spine Neck in Biochemical Compartmentalization." *Journal of Neuroscience* 20: 1722–1734.

Matsuzaki, M., N. Honkura, G. C. R. Ellis-Davies, and H. Kasai. 2004. "Structural Basis of Long-Term Potentiation in Single Dendritic Spines." *Nature* 429: 761–766.

Matus, A. 2000. "Actin-Based Plasticity in Dendritic Spines." *Science* 290: 754–758.

Megías, M., Z. Emri, T. F. Freund, and A. I. Gulyás. 2001. "Total Number and Distribution of Inhibitory and Excitatory Synapses on Hippocampal CA1 Pyramidal Cells." *Neuroscience* 102: 527–540.

Mel, B. W., J. Schiller, and P. Poirazi. 2017. "Synaptic Plasticity in Dendrites: Complications and Coping Strategies." *Current Opinion in Neurobiology* 43: 177–186.

Motley, S. E., Y. S. Grossman, W. G. M. Janssen, et al. 2018. "Selective Loss of Thin Spines in Area 7a of the Primate Intraparietal Sulcus Predicts Age-Related Working Memory Impairment." *Journal of Neuroscience* 38: 10467–10478.

Noguchi, J., M. Matsuzaki, G. C. R. Ellis-Davies, and H. Kasai. 2005. "Spine-Neck Geometry Determines NMDA Receptor-Dependent Ca2+ Signaling in Dendrites." *Neuron* 46: 609–622.

Nusser, Z., R. Lujan, G. Laube, J. D. Roberts, E. Molnar, and P. Somogyi. 1998. "Cell Type and Pathway Dependence of Synaptic AMPA Receptor Number and Variability in the Hippocampus." *Neuron* 21: 545–559.

Paxinos, G., and K. B. J. Franklin. 2004. *The Mouse Brain in Stereotaxic Coordinates: Compact Second Edition*. Gulf Professional Publishing.

Sabatini, B. L., T. G. Oertner, and K. Svoboda. 2002. "The Life Cycle of Ca (2+) Ions in Dendritic Spines." *Neuron* 33: 439–452.

Schikorski, T., and C. F. Stevens. 1999. "Quantitative Fine-Structural Analysis of Olfactory Cortical Synapses." *Proceedings of the National Academy of Sciences of the United States of America* 96: 4107–4112.

Schikorski, T., and C. F. Stevens. 2001. "Morphological Correlates of Functionally Defined Synaptic Vesicle Populations." *Nature Neuroscience* 4: 391–395.

Segal, M. 2002. "Dendritic Spines: Elementary Structural Units of Neuronal Plasticity." *Progress in Brain Research* 138: 53–59.

Spacek, J., and M. Hartmann. 1983. "Three-Dimensional Analysis of Dendritic Spines. I. Quantitative Observations Related to Dendritic Spine and Synaptic Morphology in Cerebral and Cerebellar Cortices." *Anatomy and Embryology* 167: 289–310.

Stephan, H., and O. J. Andy. 1970. "The Allocortex in Primates." In *The Primate Brain*, edited by C. R. Noback, and W. Montagna, 289–297. Appleton Century Crofts.

Tønnesen, J., G. Katona, B. Rózsa, and U. V. Nägerl. 2014. "Spine Neck Plasticity Regulates Compartmentalization of Synapses." *Nature Neuroscience* 17: 678–685.

Yuste, R. 2023. *Dendritic Spines*. 2nd ed. MIT Press.

Yuste, R., and T. Bonhoeffer. 2001. "Morphological Changes in Dendritic Spines Associated With Long-Term Synaptic Plasticity." *Annual Review of Neuroscience* 24: 1071–1089.

Yuste, R., and A. Majewska. 2001. "On the Function of Dendritic Spines." *Neuroscientist* 7: 387–395.

Supporting Information

Additional supporting information can be found online in the Supporting Information section.